

GRB Lensing Parallax: Closing Primordial Black Hole Dark Matter Mass Gap

Sunghoon Jung^{1,*} and TaeHun Kim^{1,†}

¹*Center for Theoretical Physics, Department of Physics and Astronomy, Seoul National University, Seoul 08826, Korea*

The primordial black hole (PBH) comprising full dark matter (DM) abundance is currently allowed if its mass lies between $10^{-16} M_\odot \lesssim M \lesssim 10^{-11} M_\odot$. This range is hard to be probed by gravitational lensing methods. In this paper, we revive an old discussion and advocate that the lensing parallaxes of Gamma-ray bursts (GRB) and Milky-Way (MW) stars, observed simultaneously by spatially separated detectors, can probe not only the unconstrained mass range but also the full possible range of PBH DM with lensing. The astrophysical scale accessible to us – $r_\oplus \sim \text{AU}$ – is large enough to resolve the lensing by unconstrained light PBH DM.

Introduction. The PBH has become an interesting DM candidate. Possibly having been formed from over-densities in primordial density fluctuations during inflation, it might have evaporated too much by today if it is too light or could have disturbed CMB if too heavy. A wide mass range between those general constraints remains open as DM.

PBH DM have been probed mainly by two categories: gravitational lensing and PBH-induced dynamics. The latter includes dynamical disruption, capture, and friction of observed systems, but are subject to various assumptions and uncertainties [1, 2]. Maybe the lensing is a more robust and direct probe. Among several proposals, basically only microlensing of nearby stars have been thoroughly measured, constraining $10^{-11} M_\odot \sim 10 M_\odot$ [3–7]; see also [8]. Heavier PBHs are expected to be probed by strong lensing of supernova [9]/FRB [10]/GRB and lensing fringes of GW at aLIGO [11]. On the other hand, lensing cannot efficiently probe lighter PBHs in the range $10^{-16} M_\odot - 10^{-11} M_\odot$, as lensing is typically too weak and fragile to be resolved; in particular, source size and wave-optics effects are limitations [12, 13].

In this paper, we study and advocate lensing parallaxes of GRBs and MW stars as important probes of PBH DM, with a potential to probe the whole possible mass range with lensing.

Lensing Parallax. Lensing parallax allows the detection of lensing by correlating the brightnesses (or fluxes) of a source simultaneously measured by spatially separated detectors [14]. If the spatial separation is larger than about the Einstein radius of a PBH lens, the two detectors will observe different lensing magnifications. The observed magnification of unresolved images is

$$A = \mu_1 + \mu_2 + \sqrt{\mu_1 \mu_2} \cos 2\pi c \Delta t_d / \lambda, \quad (1)$$

with each magnification

$$\mu_i = \left| \frac{1}{2} \pm (y^2 + 2) / [2y\sqrt{y^2 + 4}] \right|, \quad (2)$$

and time-dealy between images Δt_d . Eq. (2) is applicable for a point-lens and source in the geometrical optics, but will be corrected by source-size effects in final results; see below Eq. (4) and Appendix. It is this relative

angle y of a source with respect to a lens (normalized by the lens Einstein angle) that can differ between spatially separated detectors by order one, causing lensing parallax. Since the interference fringe term quickly averages out, magnification becomes $A \simeq \mu_1 + \mu_2$, frequency-independent for the majority of parameter space. Thus, different brightness with the same energy spectra between simultaneous measurements is a basic signal of lensing. However, the interference fringe (in the energy spectrum) [11, 15, 16] becomes relevant when the wavelength λ is about to be too long to probe small PBHs with mass M , i.e. $\lambda \sim \mathcal{O}(GM/c^2)$ (equivalently, $c\Delta t_d/\lambda \sim \mathcal{O}(1)$). In this regime, frequency-dependent magnification (i.e., fringe and wave-optics effects) can further strengthen lensing-parallax detection. Our study is mainly based on the former feature (frequency-independent), but the latter is also relevant near the lower mass limit.

Lensing parallax is similar to microlensing, in that brightness is measured at multiple relative angles to detect lensing. But lensing parallax can be detected even with short transients, based on *simultaneous* observations from well-separated detectors (whereas microlensing needs long-lasting sources). This allows us to use GRB pulse in lensing parallax [14]; as will be discussed, GRB is ideal to probe *lightest* unconstrained PBHs. Using pulses, we assume lensing effects do not change during measurements. The correlation can be made unambiguously between a whole time-series of pulse data, but longer temporal variation can also be cross-correlated to further strengthen the detection. The lensing parallax of long-lasting MW stars can also be detected in either way. We assume to use only short time-segment in our estimations.

Lensing parallax requires the following conditions to be met. First, the detector separation, Δr , should be larger than about the Einstein radius, r_E , of a PBH lens:

$$\Delta r \gtrsim r_E \Leftrightarrow \left(\frac{M}{10^{-7} M_\odot} \right) \lesssim \left(\frac{\Delta r}{\text{AU}} \right)^2 \left(\frac{D}{\text{Gpc}} \right)^{-1}, \quad (3)$$

where typical distance to the lens and source is denoted by $D \sim D_S \sim D_L$. A proportionality constant is not shown but varies orders of magnitudes depending on the

fractional brightness resolution ϵ , determined by Eq. (4). This condition determines the maximum PBH mass that can be probed – M_{\max} .

Second, the apparent source angular size, $\theta_S \sim r_S/D$ (where r_S is the physical transverse emission size), must be smaller than about the Einstein angle θ_E to induce sizable lensing; otherwise, only a small part of the source will be magnified. Requiring measured magnifications A_i to be more different than the resolution,

$$\delta A \equiv \frac{|A_1 - A_2|}{(A_1 + A_2)/2} \gtrsim \epsilon, \quad (4)$$

where each A_i is given by Eq. (1), and we assume to compare only two measurements for simplicity. We take into account finite source size following Ref. [17] (see also Appendix), where constant brightness profile and geometrical optics are used. The latter assumption is fine in our analysis as will be discussed; and the former, compared to profiles having a peak in the center, may slightly overestimate or underestimate the magnification depending on y . Source size r_S taken into account, the maximum magnification is $A_{\max} = \sqrt{1 + 4/\delta^2} \sim \delta A$ (for $y = 0$ in the geometrical optics) with $\delta \equiv \theta_S/\theta_E \sim r_S/r_E$. Thus, we obtain (in the limit $\delta \gtrsim 1$)

$$\left(\frac{M}{10^{-12} M_\odot} \right) \gtrsim \epsilon \left(\frac{D}{\text{Gpc}} \right)^{-1} \left(\frac{r_S}{r_\odot} \right)^2. \quad (5)$$

Eq. (4) is the main condition that we solve numerically.

Last but not least, the probe wavelength λ must be shorter than the Schwarzschild radius of a PBH lens; otherwise, the wave cannot see the lens. The geometrical optics is valid for

$$0.1 \lambda \lesssim \frac{2GM}{c^2} (1 + z_L) \simeq 10^{-5} \text{ sec} \left(\frac{M(1 + z_L)}{M_\odot} \right), \quad (6)$$

where the approximate factor 0.1 is from Ref. [18] and z_L is the lens redshift. For GRBs with $f = 10^{19} - 10^{21}$ Hz (50 keV – 5 MeV) and negligible z_L , this condition reads $M \gtrsim (10^{-15} - 10^{-17}) M_\odot$; for FRBs with $10^8 - 10^{10}$ Hz, $M \gtrsim (10^{-4} - 10^{-6}) M_\odot$; and for IR-optical observations of nearby stars with $10^{14} - 10^{16}$ Hz, $M \gtrsim (10^{-10} - 10^{-12}) M_\odot$. We will discuss later how we treat wave optics effects.

The stronger of the last two conditions (apparent source size and wavelength) determines the minimum PBH mass that can be probed – M_{\min} . The two constraints are similar for GRBs, the latter is stronger for FRBs (as radio wavelength is much longer than gamma-ray's), and the former is somewhat stronger for MW stars (as they are closer, they appear larger, and also sources are assumed to be larger).

GRB Parameters. We turn to estimate the sensitivities of GRB lensing parallax. We describe source parameters, how we treat wave-optics effects, and derive

upper limits on the PBH abundance; see Appendix for more details.

The physical transverse size r_S of emission region of GRB sources is typically correlated with the measured minimum variability time scale t_{var} as $r_S \sim ct_{\text{var}} \cdot \Gamma/(1 + z_S) \sim cT_{90}/(1 + z_S)$ [19], with the observed burst duration T_{90} , Lorentz boost Γ and source redshift z_S . Based on GRBOX database of ~ 2000 GRBs detected so far [20], 10% of GRBs have $r_S \lesssim r_\odot$; 3% have smaller $r_S \lesssim 0.1 r_\odot$; and the remaining 90% have $r_S \gtrsim r_\odot$. Although constituting a minor fraction, these smallest GRBs with $r_S \lesssim r_\odot$ are the ones that allow to probe lightest unconstrained PBH mass range. It is also notable that actual GRB sizes could be smaller; a recent work estimated smaller t_{var} based on broader GRB spectrum [21], low sampling frequency and limited photon statistics might have overestimated t_{var} [19], theoretical minimum from emission region being optically thin can also be small [12]. As a concrete example, we use the GRBOX distribution.

The GRB frequency spectrum is also relevant, as the highest frequency can probe the lightest PBHs. Rather than modeling the frequency spectrum of photon counts (which varies among GRBs) and carrying out frequency-dependent lensing analysis (needed only when Eq. (6) is not satisfied), we can simply consider a highest-frequency range where assumed sensitivity $\epsilon = 0.1$ (conservative scenario) or 0.01 (optimistic) can be typically achieved. This is a good simplification to estimate detection prospects; if the same magnification is shown at a lower-energy range (with higher flux) or if frequency-dependent magnification is observed consistent with fringe, the lensing (fringe) detection will be strengthened. But if this highest frequency range does not show evidence of lensing, detectable lensing did not occur.

Given the typical spectrum measured by Fermi GBM+LAT [22], we assume to use ~ 0.5 MeV as the highest frequency with $\epsilon = 0.1$ (conservative); this is the highest frequency where $\mathcal{O}(100)$ photon counts per MeV is typically achieved. This frequency range allows us to use geometrical optics down to $M_{\text{DM}} \gtrsim 10^{-16} M_\odot$, according to Eq. (6). In the final results, we show results only down to this mass range and defer a dedicated wave-optics study below this range. But our geometrical-optics calculation can already cover a whole unconstrained mass range. For an optimistic scenario, we assume $\epsilon = 0.01$ up to ~ 5 MeV (hence, $M_{\text{DM}} \gtrsim 10^{-17} M_\odot$). Although we use geometrical optics everywhere in this simplified analysis, we take into account source-size effects as discussed.

GRBs are at cosmological distances, observed up to $z_S \leq 10$ and majority at $z_S = 0.5 \sim 3$. We use the redshift distribution from the GRBOX database [20] to calculate lensing probability. But we do not correlate distances with observed intensities; rather, for all GRBs, we will use common intensity resolution ϵ assumed above.

	ϵ	highest frequency	N_{GRB}	Δr
conservative	0.1	~ 0.5 MeV	10^3	$2r_{\oplus}, r_{L_2}, 2\text{AU}$
optimistic	0.01	~ 5 MeV	10^4	$2r_{\oplus}, r_{L_2}, 2\text{AU}$

TABLE I. Benchmarks for GRB lensing-parallax detection. Fractional brightness resolution ϵ , the highest frequency used in our analysis, number of GRB detections N_{GRB} , and detector separation Δr . For MW stars, $N_{\text{star}} = 10^7$ and 10^9 .

Benchmark detector separations are $\Delta r = 2r_{\oplus} \simeq 0.04$ sec, $r_{L_2} \simeq 5$ sec, and $2 \text{ AU} \simeq 10^3$ sec. The first choice is based on telescopes on the ground and low Earth orbits such as Fermi and Swift; the second may be possible as IR-band space missions such as Gaia, WFIRST and Euclid are operating or planned on orbits around the Lagrange point L_2 of the Sun-Earth system; and the AU is a characteristic scale of the solar system, as is realized in Kepler mission. The detection benchmarks are summarized in Table. I.

Results. The optical depth, τ , is obtained from the volume of the desired PBH locations (for the given GRB) that can lead to appreciable lensing parallax; then the expected number of PBHs within this volume is the optical depth. PBHs are assumed to be uniformly distributed with the comoving number density $n = \rho_{\text{crit},0}\Omega_{\text{DM}}f/M$, where $f \equiv \Omega_{\text{PBH}}/\Omega_{\text{DM}}$ is the PBH abundance. As shown in Fig. 2, $\tau \gtrsim 10^{-2}$ is sizable for the majority of GRBs at $z = 0.5 \sim 3$ and unconstrained PBH masses. But what is relevant to lensing parallax is the single-lensing probability, not multiple lensings of a source which may complicate the detection. The single-lensing probability is $P_1 = \tau e^{-\tau}$ for the Poisson distribution of lenses and becomes its maximum 0.37 at $\tau = 1$. Thus, one can expect many GRB lensing parallaxes.

In Fig. 1, we obtain 95% CL upper limits on the PBH abundance by assuming that no lensing parallax will be detected among total $N_{\text{GRB}} = 1000$ (as already more than this) or 10^4 GRBs simultaneously observed by Δr -separated detectors. The Poisson distribution of the number of lenses is used. In each of conservative and optimistic projections, three benchmark results with Δr are shown. As discussed, we plot results down to the lowest mass where geometrical optics is valid for the highest-frequency range that we consider.

One can first understand overall behaviors of the results. The three Δr lines have similar M_{min} as it is determined dominantly by ϵ and r_S ; $M_{\text{min}} \sim 10^{-15} - 10^{-16} M_{\odot}$ is indeed expected from Eq. (5) with $\epsilon = 0.1$, $r_S \lesssim 0.1 r_{\odot}$, and $D \sim 1$ Gpc. Optimistic results improve $M_{\text{min}} \propto \epsilon$ with higher frequencies available. But the three lines have different $M_{\text{max}} \propto (\Delta r)^2$ (Eq. (3)). The constraints on f is also improved roughly with the increase of N_{GRB}/ϵ , yielding higher statistics.

As a result, the unconstrained PBH DM mass range $-10^{-16} M_{\odot} \lesssim M \lesssim 10^{-11} M_{\odot}$ – can be potentially

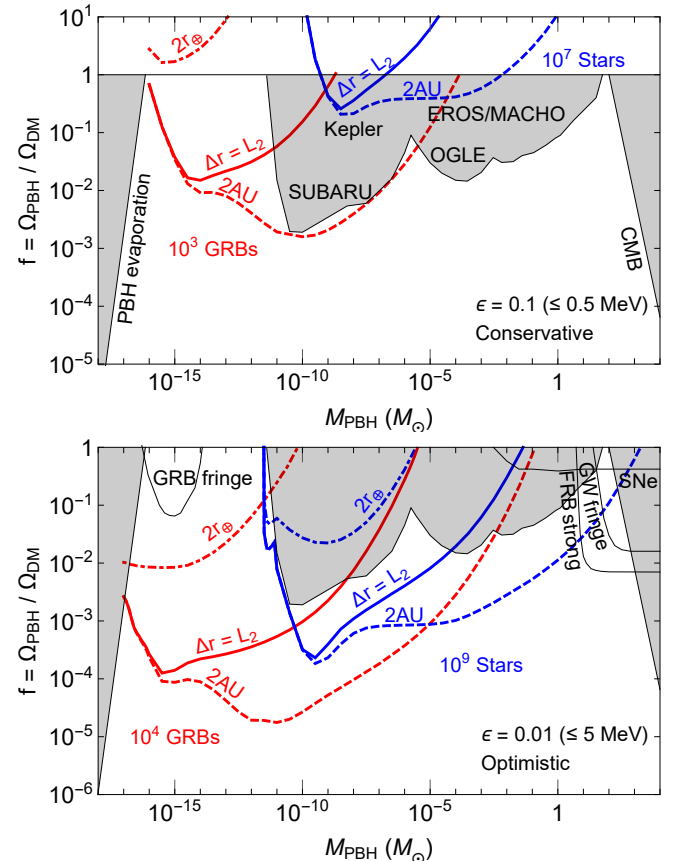


FIG. 1. Expected 95% CL upper limits on the PBH abundance, f , from lensing parallaxes of GRB(red) and MW star(blue). The upper and lower panels show conservative and optimistic projections with detection benchmarks in Table I. The region with $f > 1$ is not possible but is shown for reference. Also shown are existing(shaded) and proposed(non-shaded) lensing constraints from microlensing (SUBARU [3], Kepler [5], OGLE/EROS/MACHO [4, 6, 7]), strong lensing of FRB [10]/supernova [9], GW fringe (aLIGO) [11], and GRB fringe [12]; evaporation of too light PBHs [23], and CMB distortion from too heavy ones [24]. In all, the full range of possible PBH DM mass can be probed by lensing.

probed by lensing. Existing telescopes (having conservative specs while running on the ground and low Earth orbits) alone can barely achieve sensitivities yet; see $\Delta r = 2r_{\oplus}$ result. But, remarkably, one space telescope at a larger orbit (L_2 or AU), paired with existing ones, can be enough to probe a whole unconstrained mass range; see $\Delta r = r_{L_2}$ and 2AU results. With optimistic benchmarks, any combinations of well-separated detectors (even low-orbit ones) can probe the whole unconstrained mass range.

Confidently probing the lightest mass range near $10^{-16} M_{\odot}$ likely requires improvements from the conservative scenario; in particular, better resolution $\epsilon < 0.1$. Such can perhaps be achieved with higher photon counting rates from larger detector area, higher sampling fre-

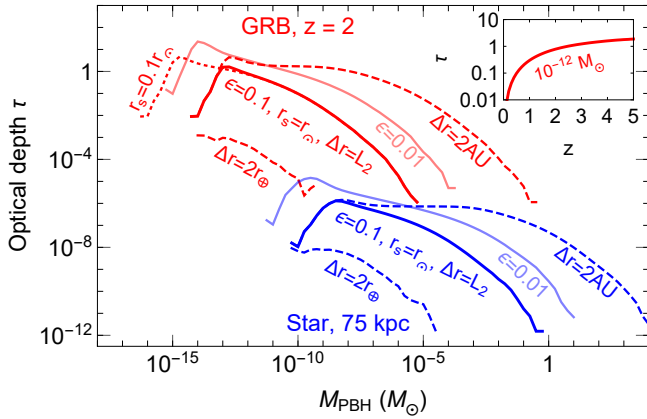


FIG. 2. Optical depth τ for the lensing parallax of GRB(red) at $z_S = 2$ and MW-star(blue) at 75 kpc. The inset shows the z_S -dependence for $M = 10^{-12} M_\odot$ as a reference. Uniform PBH distribution is used.

quency, and better detection efficiency. GRB source size is also a key factor (Eq. (5)) as recently emphasized for GRB fringes [12] (their result with $10^4 \times 3\% = 300$ GRBs with $r_S = 10^9$ cm [12] is shown in Fig. 1). If sources turn out to be larger than the estimate used here, much better ϵ is needed.

Toward the heaviest mass range, GRB lensing parallax can probe potentially up to $M \lesssim 0.1 M_\odot$. In the heavier mass range, various strong and microlensing observables are available, as shown in Fig. 1. Supernova lensing magnification can be detected as a deviation in the brightness-redshift relation (result with current data is shown [9]); FRB and GRB pulses can be strongly time-delayed or angular separated (10^4 FRBs up to $z \leq 0.5$ [10]); and GW lensing fringes in chirping waveforms can be detected at aLIGO ($\sim 10^3$ mergers for 1 yr [11]) probing the mass range corresponding to the LIGO frequency band.

Milky-Way Stars. Stars in Milky-Way and nearby galaxies – that we collectively call by MW stars – are another interesting candidates of lensing parallax. Many of them are obviously small solar sizes while much closer to us, efficiently probing a different mass range.

We simply assume that all MW stars have $r_S = r_\odot$ and use geometrical optics. We consider 10^7 (as in current microlensings) or 10^9 MW stars observed, uniformly distributed within a 100 kpc sphere around us. Such a large number of sources can compensate the small optical depth ($\tau \lesssim 10^{-5}$ shown in Fig. 2, similar to microlensing values [3]). As for lenses, we assume that PBHs with mass M comprise the total MW mass $10^{12} M_\odot$, uniformly distributed within a 100 kpc sphere around us, simplifying the DM halo of the MW.

Although stars are long-lasting, we assume to consider short time-segments as discussed; but annual parallaxes in the usual microlensing has been indeed stud-

ied, e.g. [25, 26]. We simply require the same lensing-detection criteria and benchmarks as in the GRB case; but prospects for realizing various Δr and good resolution ϵ are higher here, as various IR-band space missions are already operating with such specs or planned to be achieving them.

The sensitivities are overlapped in Fig. 1. MW stars are sensitive to heavier PBHs; as they are closer than GRBs, they appear larger and the Einstein radius of a PBH is smaller. Compared to GRBs, M_{\max} is larger by roughly $(1 \text{ Gpc}/100 \text{ kpc}) \sim 10^4$ (see Eq. (3)) while M_{\min} is larger by $\sim 10^5 - 10^6$ as no smaller stars are assumed. Notably, ongoing and proposed missions on the ground and in large orbits (L_2 or AU) can already achieve any of conservative results, probing $10^{-9} M_\odot \lesssim M \lesssim 10^{-2} M_\odot$. Optimistically, $10^{-12} M_\odot \lesssim M \lesssim 10^3 M_\odot$ can all be probed, complementary to microlensing and strong lensing.

Discussion. GRB has several advantages in completing the lensing probe of PBH DM. Being at cosmological distances, it can probe PBH DM in a large volume of the Universe, not just in our neighborhood. The large distance, compact source, and high-frequency gamma rays all combined make it appropriate to probe the lightest mass range. The high-frequency also makes it insusceptible to intergalactic scattering dispersion, one of the main limiting factors for FRB fringes [27]. Compared with lensing fringe (e.g. GRB fringe also known as femtolensing, shown in Fig. 1), intensity correlation relaxes the source-size constraint and hence probes a much wider mass range. Lensing parallax from simultaneous measurements allows all these possible with GRB pulses.

In all, the full range of PBH DM mass can be probed by lensing. GRB lensing parallax can probe the unconstrained lightest mass range, while MW-star lensing parallax can probe a heavier range complementary to existing lensing observables. The maximum mass range is determined by detector separation, while the minimum range depends crucially on GRB source size $\lesssim r_\odot$, spectrum above 0.1 MeV, and brightness resolution $\epsilon \lesssim 0.1$. Remarkably, even a single gamma-ray space telescope at an L_2 or AU-sized orbit with current sensitivities (conservative $\Delta r = r_{L_2}, 2\text{AU}$ results in Fig. 1) will be good enough to accomplish this probe. Fortunately, the astrophysical scale accessible to us – from r_\oplus to AU – is just right to probe the allowed (and unconstrained) PBH mass range.

Acknowledgements. Authors would like to thank Myungshin Im, Ji-hoon Kim, and Sascha Trippe for useful discussions. Authors are supported by Grant Korea NRF-2019R1C1C1010050, 2015R1A4A1042542, and SJ also by POSCO Science Fellowship.

APPENDIX

1. Useful numbers and formulas. Here we present some useful numbers and formulas, with $c = 1$.

Cosmological constants we assumed are

$$H_0 = 70 \text{ km/s/Mpc}, \quad (7a)$$

$$\rho_{crit,0} = \frac{3H_0^2}{8\pi G} = 9.21 \times 10^{-27} \text{ kg/m}^3 \\ = 1.36 \times 10^{11} M_\odot/\text{Mpc}^3, \quad (7b)$$

$$\Omega_\Lambda = 0.7, \Omega_r = 0, \Omega_M = 0.3, \Omega_{DM} = 0.26. \quad (7c)$$

Representative lengths are

$$r_\oplus \simeq 0.02 \text{ sec}, \quad r_\odot \simeq 2 \text{ sec}, \quad r_{L_2} \simeq 5 \text{ sec}, \\ \text{AU} \simeq 500 \text{ sec}. \quad (8)$$

The Einstein radius of a PBH is

$$r_E \simeq 1.4 \times 10^6 \text{ sec} \sqrt{\left(\frac{M}{M_\odot}\right) \left(\frac{D}{\text{Gpc}}\right)}. \quad (9)$$

The Schwarzschild radius is

$$r_{\text{Sch}} \simeq 10^{-5} \text{ sec} \left(\frac{M}{M_\odot}\right). \quad (10)$$

Time delay is

$$\Delta t_d \sim 2 \times 10^{-5} \text{ sec} \left(\frac{M}{M_\odot}\right). \quad (11)$$

2. Finite source-size effect. We present the equation for the magnification A that we used in the calculation, with finite source-size considered.

Magnification of a finite sized circular source with constant surface brightness by a point-lens in the geometrical optics limit is given by [17]

$$A(y, \delta) \approx \begin{cases} A_{in}(y, \delta) & \text{for } y < \delta, \\ A_{out}(y, \delta) & \text{for } y > \delta, \end{cases} \quad (12)$$

where

$$A_{in}(y, \delta) = \sqrt{1 + \frac{4}{\delta^2}} - \frac{8}{\delta^3(\delta^2 + 4)^{3/2}} \frac{y^2}{2} \\ - \frac{144(\delta^4 + 2\delta^2 + 2) y^4}{\delta^5(\delta^2 + 4)^{7/2}} \frac{24}{24}, \quad (13a)$$

$$A_{out}(y, \delta) = \frac{2 + y^2}{y\sqrt{y^2 + 4}} + \frac{8(y^2 + 1)}{y^3(y^2 + 4)^{5/2}} \frac{\delta^2}{2} \\ + \frac{48(3y^6 + 6y^4 + 14y^2 + 12)}{y^5(y^2 + 4)^{9/2}} \frac{\delta^4}{24}. \quad (13b)$$

Near $y \approx \delta$, y_{in} and y_{out} over- and underestimates the magnification compared to the actual value, respectively. In our calculation, we used each equation in $y \leq 0.9\delta$ and

$y \geq 1.1\delta$ respectively, and then linearly interpolated the magnification in $0.9\delta < y < 1.1\delta$.

3. Computing optical depth and constraints.

Here we explain our computational procedure for the optical depths and the bounds on the PBH abundance.

We assumed a uniform distribution of PBHs with number density n , so the optical depth for a source of physical transverse size r_S at comoving distance χ_S is given by

$$\tau(\chi_S; f; M; \Delta r_\perp, r_S, \epsilon) \\ = n(f; M) \times V_L(\chi_S; \Delta r_\perp, r_S, \epsilon), \quad (14)$$

where V_L is the desired comoving volume for PBHs and $\Delta r_\perp = \Delta r \cos \theta$ is the component of Δr perpendicular to the line-of-sights (LOSs). The volume V_L is given by

$$V_L(\chi_S; \Delta r_\perp, r_S, \epsilon) = \int_0^{\chi_S} \sigma(\chi_L; \Delta r_\perp, r_S, \epsilon) d\chi_L \quad (15)$$

where σ is the comoving cross-section for the lensing-detection of PBH at comoving distance χ_L . Since the universe is flat, we do not distinguish the transverse comoving distance from the usual LOS comoving distance.

To calculate σ , we first draw a region on the lens plane that at least one of the A_1 or A_2 exceeds $1 + \epsilon$ (the necessary condition for Eq. (4)). Then we draw a rectangular region circumscribing the previous one, and divide into 6400 equal-sized rectangular sectors (80 divisions for each edge). Next, we check whether Eq. (4) is satisfied at the center of each sector, and summing up the area of the relevant sectors gives σ .

Going back to equation (15), we equally divided the χ_L range into 24 sectors and used the midpoint quadrature for the integral. Finally, multiplying it by n gives the optical depth τ . Note that the only dependence on f comes from $n \propto f$, so single evaluation of τ at $f = 1$ immediately gives $\tau(f)$.

Now we move onto the bound calculation. The probability of having no detection for observing N sources is given by $P_{\text{null}}(f) = \prod_{i=1}^N (1 - P_{1,i}(f))$, where i is the source index. The bound of f is the one which gives $P_{\text{null}}(f) = 0.05$. In the actual calculation, we sample 1000 sources, with distance and source size randomly selected according to the distributions given by Fig. 4 and with purely random angular positions. We approximated P_{null} by assuming that each sampled source represents $N/1000$ observations, giving $P_{\text{null}}(f) \approx \prod_{i=1}^{1000} (1 - P_{1,i}(f))^{N/1000}$.

4. Single lensing with PBH clustering. We now demonstrate that assuming a uniform distribution of PBHs is decent in calculating the bound of PBH abundance, even though the actual PBHs are thought to be clustered around galaxies. We derive the single lensing probability P_1 in clumpy distribution, check how it depends on relevant parameters, estimate those parameters in our cases, and finally conclude that the previously obtained bounds are still valid in realistic distributions.

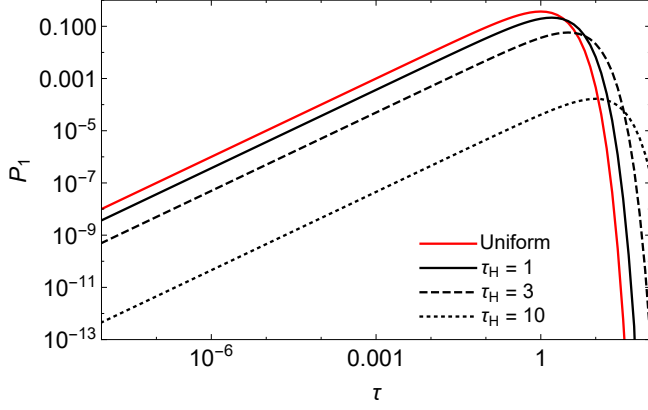


FIG. 3. Single lensing probability P_1 as a function of optical depth, for several selected τ_H 's. The larger τ_H means that the halo is more clustered so that the optical depth inside a single halo is larger. The red line is for the uniform distribution of PBHs giving the Poisson distribution, while black lines represent clumped distributions which depart from the Poisson distribution.

First, we note that the optical depth τ for GRB is not affected by the clustering. However, the number of lenses in V_L will no more follow the Poisson distribution. As lenses are clustered, there are more chances for V_L to avoid the lenses by not intersecting the halos. On the other hand, once it meets a halo, the high number density inside it could promote multiple lensings.

The above argument implies that P_1 depends on the expected number of lenses getting into V_L when it intersects a single halo. This shall be denoted by τ_H . Then the expected number of relevant halos is given by $\langle N \rangle = \tau/\tau_H$. For simplicity, we assume the halos are uniformly distributed over the universe, while PBHs are also uniformly distributed inside each halo. Then both N and the number of relevant lenses inside one relevant halo follow Poisson distributions. We can calculate the conditional probability to have a single lensing when there are N relevant halos as

$$\begin{aligned}
 & P_{1|N \text{ halos}} \\
 &= (\text{number of cases to choose one halo for lensing}) \\
 & \quad \times (\text{probability for that halo giving single lensing}) \\
 & \quad \times (\text{probability for other halos giving no lensing}) \\
 &= N \times \tau_H e^{-\tau_H} \times (e^{-\tau_H})^{N-1}, \tag{16}
 \end{aligned}$$

so the total probability for single lensing is

$$P_1 = \sum_{N=1}^{\infty} P_{1|N \text{ halos}} \times \frac{(\tau/\tau_H)^N}{N!} e^{-\tau/\tau_H}. \tag{17}$$

Figure 3 shows P_1 as a function of τ for three selected τ_H 's. The deviation from the Poisson distribution certainly depends on τ_H ; it diminishes for $\tau_H \lesssim 1$, while $\tau_H \gtrsim 1$ gives meaningful deviation.

Now, the bounds will be eased by the same factor as the decrement of P_1 , which is decided by τ_H . So the next step is estimating τ_H . From the assumed uniform distribution of PBHs inside each halo, $\tau_H = n_{|H} \times V_{\sigma|H}$, where $n_{|H}$ is the internal lens number density and $V_{\sigma|H}$ is the lensing-relevant volume (equivalent to the volume covered by σ) for one halo. For a halo mass M_H and radius R_H , $n_{|H} = (M_H f/M)/(4/3 \times \pi R_H^3)$. For $V_{\sigma|H}$, we express $\sigma = k \cdot \pi (D_L \theta_E)^2$, where k can be larger than 1 if ϵ is small so that lensing cross section is large. This gives in average $V_{\sigma|H} = 4/3 \times R_H k \pi (D_L \theta_E)^2$. This gives

$$\tau_H \approx 1.9 \times 10^{-22} \times kf \left(\frac{M_H}{M_\odot} \right) \left(\frac{D_L}{R_H} \right)^2 \left(\frac{1 \text{ Gpc}}{D_L D_S / D_{LS}} \right). \tag{18}$$

For our cases, halos are at cosmological distances so D 's are all ~ 1 Gpc (note that D is the angular diameter distance), and we assume a MW-like halo of $M_H = 10^{12} M_\odot$ and $R_H \sim 100$ kpc. For k , it could reach up to $k \approx 70$, but usually $k \lesssim 10$ for the most of values of M or ϵ . Lastly for f , we use the bound values in Fig. 1. So here we are checking whether the effect of the clustering on the bounds can be regarded as a small perturbation. We choose a fiducial value $f = 10^{-2}$, a typical value for the conservative bounds and a relatively weak value for the optimistic ones.

Using all these values, we get $\tau_H \lesssim 2 \times 10^{-3}$. Fig. 3 implies that this would barely give difference on P_1 , and hence the bounds are firm.

Let us finally estimate the value of R_H that induces a meaningful difference on the bounds, say, eased by a factor 2. This requires P_1 to decrease by a half, which needs $\tau_H \approx 0.7$. Comparing with the former values, the $1/R_H^2$ dependence of τ_H gives $R_H \lesssim 5$ kpc (with the uniform distribution of PBHs; incorporating more realistic DM distributions is beyond the scope of our paper). This is an unnaturally small size. Thus, we again conclude that our bounds are valid also in clumpy distributions of PBHs.

5. GRB source parameter distribution. Finally, we present the distributions for GRB redshifts and transverse sizes that we use.

The GRB data on [20] were used to obtain the redshift and the transverse size distributions for observed GRBs. Out of 2105 GRB observations, 487 have redshift information and 1944 have T_{90} information which is converted to the transverse size by $r_S \sim c \times T_{90}$ [19].

Figure 4 shows the redshift and transverse size distribution of observed GRBs. For the redshift distribution, the population extends to very high redshifts of $z \leq 10$, but the majority of the population lies in $z \lesssim 3$. For the transverse size distribution, the bimodal distribution is shown while the majority of the population lies in $r_S \geq r_\odot$. Out of 1944 GRBs with transverse size converted from T_{90} , 226 (12%) have $r_S \leq r_\odot$ and only 58 (3%) among them satisfies $r_S \leq 0.1r_\odot$. These fractions

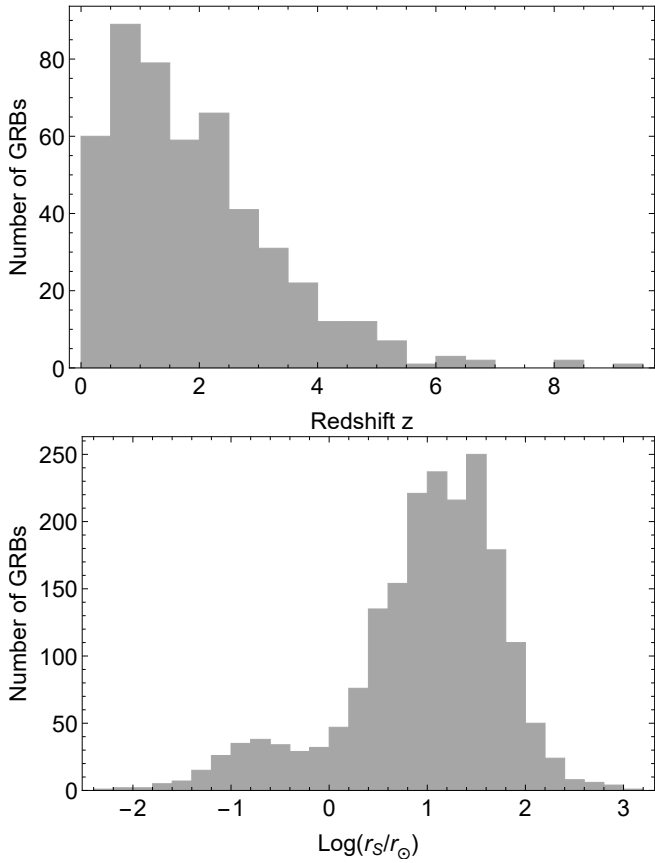


FIG. 4. Histograms of redshift (upper panel) and transverse size (lower panel) of observed GRBs that we use. Using a total of 2105 observed GRB data in [20], the redshift distribution was obtained from 487 GRBs with redshift information, and the transverse size distribution was obtained from 1944 GRBs with T_{90} information that further converted by $r_S \sim c \times T_{90}$.

are smaller than the analysis done in [12, 21], estimating about 10% of observed GRBs have $r_S \leq 0.1r_\odot$. Although the proper transverse size should be estimated by $T_{90}/(1 + z_S)$, we omitted the redshift factor in calculating the size distribution to be conservative for unknown redshifts of the majority of GRBs used in obtaining the transverse size distribution.

* sunghoonj@snu.ac.kr

† gimthcha@snu.ac.kr

- [1] B. Carr, F. Kuhnel and M. Sandstad, “Primordial Black Holes as Dark Matter,” *Phys. Rev. D* **94**, no. 8, 083504 (2016) doi:10.1103/PhysRevD.94.083504 [arXiv:1607.06077 [astro-ph.CO]].
- [2] M. Sasaki, T. Suyama, T. Tanaka and S. Yokoyama, “Primordial black holes perspectives in gravitational wave astronomy,” *Class. Quant. Grav.* **35**, no. 6, 063001 (2018) doi:10.1088/1361-6382/aaa7b4 [arXiv:1801.05235 [astro-ph.CO]].
- [3] H. Niikura *et al.*, “Microlensing constraints on primordial

- black holes with Subaru/HSC Andromeda observations,” *Nat. Astron.* **3**, no. 6, 524 (2019) doi:10.1038/s41550-019-0723-1 [arXiv:1701.02151 [astro-ph.CO]].
- [4] H. Niikura, M. Takada, S. Yokoyama, T. Sumi and S. Masaki, “Constraints on Earth-mass primordial black holes from OGLE 5-year microlensing events,” *Phys. Rev. D* **99**, no. 8, 083503 (2019) doi:10.1103/PhysRevD.99.083503 [arXiv:1901.07120 [astro-ph.CO]].
- [5] K. Griest, A. M. Cieplak and M. J. Lehner, *Astrophys. J.* **786**, no. 2, 158 (2014) doi:10.1088/0004-637X/786/2/158 [arXiv:1307.5798 [astro-ph.CO]].
- [6] P. Tisserand *et al.* [EROS-2 Collaboration], *Astron. Astrophys.* **469**, 387 (2007) doi:10.1051/0004-6361:20066017 [astro-ph/0607207].
- [7] R. A. Allsman *et al.* [Macho Collaboration], *Astrophys. J.* **550**, L169 (2001) doi:10.1086/319636 [astro-ph/0011506].
- [8] J. A. Dror, H. Ramani, T. Trickle and K. M. Zurek, “Pulsar Timing Probes of Primordial Black Holes and Subhalos,” *Phys. Rev. D* **100**, no. 2, 023003 (2019) doi:10.1103/PhysRevD.100.023003 [arXiv:1901.04490 [astro-ph.CO]].
- [9] M. Zumalacarregui and U. Seljak, “Limits on stellar-mass compact objects as dark matter from gravitational lensing of type Ia supernovae,” *Phys. Rev. Lett.* **121**, no. 14, 141101 (2018) doi:10.1103/PhysRevLett.121.141101 [arXiv:1712.02240 [astro-ph.CO]].
- [10] J. B. Muoz, E. D. Kovetz, L. Dai and M. Kamionkowski, “Lensing of Fast Radio Bursts as a Probe of Compact Dark Matter,” *Phys. Rev. Lett.* **117**, no. 9, 091301 (2016) doi:10.1103/PhysRevLett.117.091301 [arXiv:1605.00008 [astro-ph.CO]].
- [11] S. Jung and C. S. Shin, “Gravitational-Wave Fringes at LIGO: Detecting Compact Dark Matter by Gravitational Lensing,” *Phys. Rev. Lett.* **122**, no. 4, 041103 (2019) doi:10.1103/PhysRevLett.122.041103 [arXiv:1712.01396 [astro-ph.CO]].
- [12] A. Katz, J. Kopp, S. Sibiryakov and W. Xue, “Femtolensing by Dark Matter Revisited,” *JCAP* **1812**, 005 (2018) doi:10.1088/1475-7516/2018/12/005 [arXiv:1807.11495 [astro-ph.CO]].
- [13] Y. Bai and N. Orlofsky, “Microlensing of X-ray Pulsars: a Method to Detect Primordial Black Hole Dark Matter,” *Phys. Rev. D* **99**, no. 12, 123019 (2019) doi:10.1103/PhysRevD.99.123019 [arXiv:1812.01427 [astro-ph.HE]].
- [14] R. J. Nemiroff and A. Gould, “Probing for MACHOs of mass $10^{-15}M_\odot$ – $10^{-7}M_\odot$ with gamma-ray burst parallax spacecraft,” *Astrophys. J.* **452**, L111 (1995) doi:10.1086/309722 [astro-ph/9505019].
- [15] A. Gould, “Femtolensing of gamma-ray bursters,” *Astrophys. J.* **386**, L5 (1992) doi:10.1086/186279
- [16] T. T. Nakamura, “Gravitational lensing of gravitational waves from inspiraling binaries by a point mass lens,” *Phys. Rev. Lett.* **80**, 1138 (1998). doi:10.1103/PhysRevLett.80.1138
- [17] H. J. Witt and S. Mao, “Can lensed stars be regarded as pointlike for microlensing by MACHOs?,” *Astrophys. J.* **430**, no. 2, 505 (1994) doi:10.1086/174426
- [18] R. Takahashi and T. Nakamura, “Wave effects in gravitational lensing of gravitational waves from chirping binaries,” *Astrophys. J.* **595**, 1039 (2003) doi:10.1086/377430 [astro-ph/0305055].

- [19] A. Barnacka and A. Loeb, “A size-duration trend for gamma-ray burst progenitors,” *Astrophys. J.* **794**, no. 1, L8 (2014) doi:10.1088/2041-8205/794/1/L8 [arXiv:1409.1232 [astro-ph.HE]].
- [20] <http://www.astro.caltech.edu/grbox/grbox.php>
- [21] V. Z. Golkhou, N. R. Butler and O. M. Littlejohns, “The Energy-Dependence of GRB Minimum Variability Timescales,” *Astrophys. J.* **811**, no. 2, 93 (2015) doi:10.1088/0004-637X/811/2/93 [arXiv:1501.05948 [astro-ph.HE]].
- [22] https://fermi.gsfc.nasa.gov/ssc/data/analysis/documentation/Cicerone/Cicerone_GRBs/Overview_GRB_Spec_Anal.html
The shown typical spectrum peaks at $\mathcal{O}(100)$ keV with energy flux ~ 1 MeV cm^{-2} sec^{-1} ; a typo in the unit is corrected here. With 100 cm^2 Fermi detector area, $\mathcal{O}(100)$ photon counts per MeV is typically achieved at $\mathcal{O}(100)$ keV.
- [23] B. J. Carr, K. Kohri, Y. Sendouda and J. Yokoyama, *Phys. Rev. D* **81**, 104019 (2010) doi:10.1103/PhysRevD.81.104019 [arXiv:0912.5297 [astro-ph.CO]].
- [24] Y. Ali-Hamoud and M. Kamionkowski, *Phys. Rev. D* **95**, no. 4, 043534 (2017) doi:10.1103/PhysRevD.95.043534 [arXiv:1612.05644 [astro-ph.CO]].
- [25] B. Grieger, R. Kayser, S. Refsdal, “A parallax effect due to gravitational micro-lensing,” *Nature* **324**, 126 (1986) doi:10.1038/324126a0.
- [26] E. Bachelet, T. C. Hinse, R. Street, “Measuring the Microlensing Parallax from Various Space Observatories,” *Astrophys. J.* **155**, no. 5, 7 (2018) doi:10.3847/1538-3881/aab3c8 [arXiv:1803.00689 [astro-ph.EP]].
- [27] Z. Zheng, E. O. Ofek, S. R. Kulkarni, J. D. Neill and M. Juric, *Astrophys. J.* **797**, no. 1, 71 (2014) doi:10.1088/0004-637X/797/1/71 [arXiv:1409.3244 [astro-ph.HE]].